Journal of Volcanology and Geothermal Research 291 (2015) 72–85

Contents lists available at ScienceDirect

Journal of Volcanology and Geothermal Research

journal homepage: www.elsevier.com/locate/jvolgeores

Composite volcanoes in the south-eastern part of İzmir–Balıkesir Transfer Zone, Western Anatolia, Turkey

Ioan Seghedi [a], Cahit Helvacı [b], Zoltan Pécskay [c]

[a] Institute of Geodynamics, Romanian Academy, Jean-Louis Calderon 19-21, Bucharest 020032, Romania
[b] Dokuz Eylül Üniversitesi, Mühendislik Fakültesi, Jeoloji Mühendisliği Bölümü, TR-35160 İzmir, Turkey
[c] Institute of Nuclear Research, Hungarian Academy of Sciences, P.O. Box 51, Bem ter 18/c, H-4001, Debrecen, Hungary

ARTICLE INFO

Article history:
Received 9 September 2014
Accepted 28 December 2014
Available online 9 January 2015

Keywords:
Western Anatolia
İzmir–Balıkesir Transfer Zone
Volcanology
K/Ar age
Geochemistry
Miocene volcanism

ABSTRACT

During the Early–Middle Miocene (Western Anatolia) several volcanic fields occur along a NE–SW-trending shear zone, known as İzmir–Balıkesir Transfer Zone. This is a deformed crustal-scale sinistral strike-slip fault zone crossing the Bornova flysch and extending along the NW-boundary of the Menderes Massif by accommodating the differential deformation between the Cycladic and Menderes core complexes within the Aegean extensional system. Here we discuss the volcanic activity in Yamanlar and Yuntdağı fields that is closely related to the extensional tectonics of the İzmir–Balıkesir Transfer Zone and in the same time with the episodic core complex denudation of the Menderes Massif.

This study documents two composite volcanoes (Yamanlar and Yuntdağı), whose present vent area is strongly eroded and cut by a variety of strike-slip and normal fault systems, the transcurrent NW–SE being the dominant one. The erosional remnants of the vent areas, resembling a shallow crater intrusive complex, illustrate the presence of numerous dykes or variably sized neck-like intrusions and lava flows, typically associated with hydrothermal alteration processes (propylitic and argillic). Such vent areas were observed in both the examined volcanic fields, having ~6 km in diameter and being much more eroded toward the south, along the NW–SE fault system. Lava flows and lava domes are sometimes associated with proximal block and ash flow deposits. In the cone-building association part, besides lava flows and remnants of lava domes, rare block and ash and pumice-rich pyroclastic flow deposits, as well as a series of debris-flow deposits, have been observed.

The rocks display a porphyritic texture and contain various proportions of plagioclase, clinopyroxene, orthopyroxene, amphibole, rare biotite and corroded quartz. The examined rocks fall at the limit between calc-alkaline to alkaline field, and plot predominantly in high-K andesite and dacite fields and one is rhyolite. The trace element distribution suggests fractional crystallization processes and mixing in upper crustal magma chambers and suggests a metasomatized lithospheric mantle/lower crust source. This preliminary volcanological–petrological and geochronological base study allowed documenting the Yamanlar and Yuntdağı as composite volcanoes generated during post-collisional Early–Middle Miocene transtensional tectonic movements.

1. Introduction

Western Anatolia is characterized by two main continental assemblages known as the Sakarya micro-plate to the north and the Anatolide–Tauride block to the south. These terranes were amalgamated during Late Cretaceous–Paleocene continental collision along the northern branch of the Neo-Tethys, which is marked by the Vardar–İzmir–Ankara Suture Zone (see inset Fig. 1). The rocks of the Vardar–İzmir–Ankara Suture Zone in western Anatolia are represented by the ophiolitic mélange units of the Bornova Flysch Zone and Tavşanlı Zone. Widespread orogenic magmatic activity developed in the Western Anatolian Volcanic Province from the Eocene to Miocene (e.g., Helvacı et al., 2009; Ersoy and Palmer, 2013; Göktaş, 2014). The exhumation of the Menderes Massif along the crustal-scale low-angle detachment faults was accompanied by NE–SW-trending high-angle strike-slip faults along its western and eastern margins (Erkül et al., 2005a; Ersoy et al., 2011, 2012a; Erkül, 2012; Erkül and Erkül, 2012; Karaoğlu and Helvacı, 2012b). The NE–SW-trending zone of deformation along the western margin of the Menderes Core Complex is termed the İzmir–Balıkesir Transfer zone (İBTZ) (Erkül et al., 2005a; Uzel and Sözbilir, 2008; Ersoy et al., 2011, 2012b; Karaoğlu, 2014). The İBTZ represents the NE extension into west Turkey of a NE–SW-trending crustal-scale shear zone (the mid-Cycladic lineament), along which Miocene granitoids were emplaced in the Cyclades (Pe-Piper et al., 2002). The NE–SW-trending high-angle strike-slip faults are recorded

E-mail address: seghedi@geodin.ro (I. Seghedi).

http://dx.doi.org/10.1016/j.jvolgeores.2014.12.019
0377-0273/

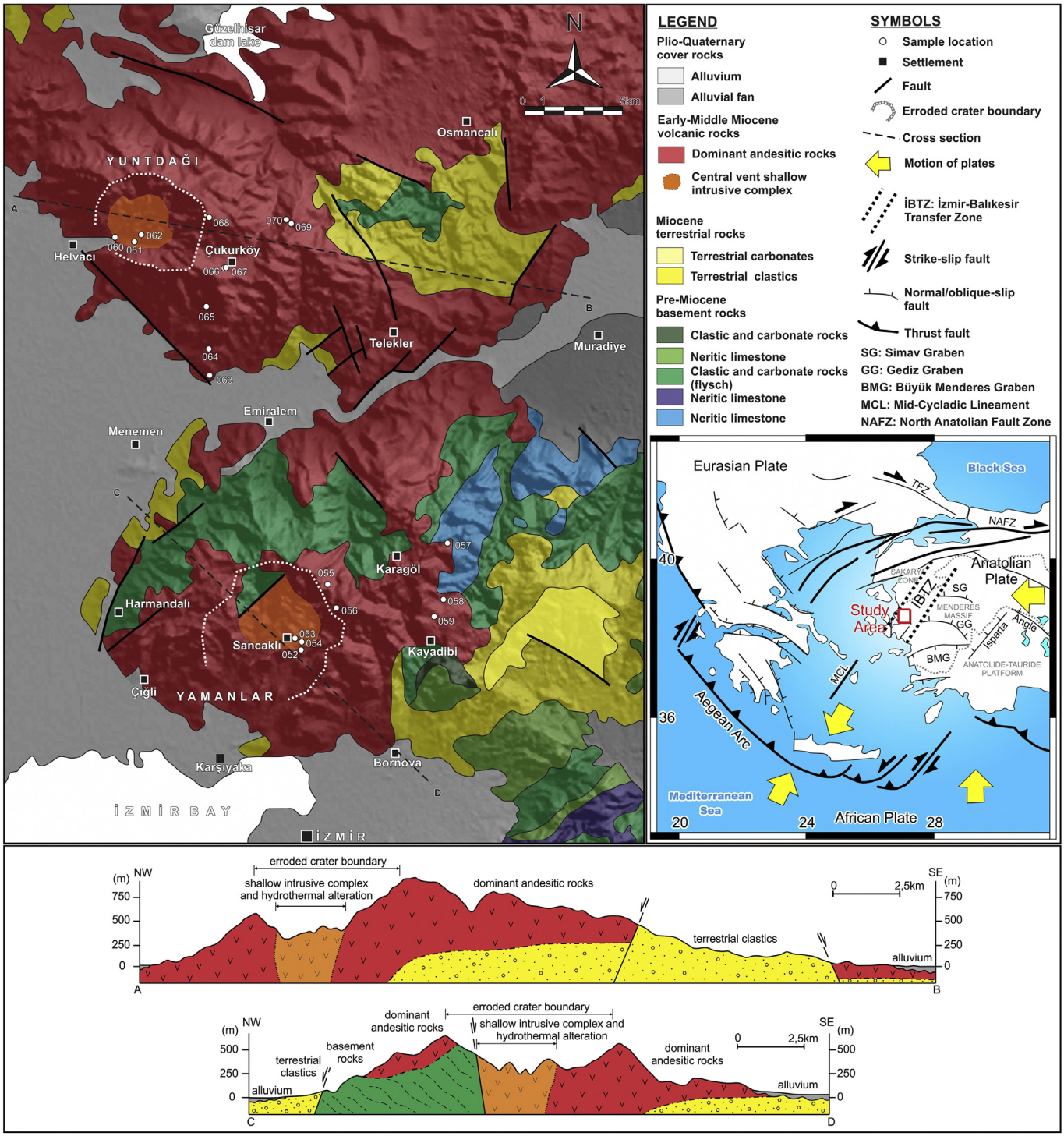

Fig. 1. Geological map of the study area and two simplified profiles, each crossing the crater areas of Yamanlar and Yuntdağı volcanoes (modified from MTA Geological maps, 1/100 000 Scale). The inset is showing the study area situated at the south-western part of İzmir–Balıkesir transfer zone and the edge with Menderes Core Complex.

in several Neogene basins, such as along the eastern margins of the NE–SW-trending Kocaçay (Sözbilir et al., 2011), Kocaçay and Cumaovası basins (Kayseri-Özer et al., 2014) and Gördes basins (Ersoy et al., 2011). (Fig. 2)

Composite volcanoes are essentially confined to a single vent or a group of closely spaced central vents showing a simple conical or shield-like overall symmetry and having more than one evolutionary stage in their existence (e.g. Francis, 1993). Such volcanoes have been dominantly found associated with arc volcanism and subduction processes, or post-collisional processes (e.g. Lexa et al., 2010). Here, we discuss for the first time two composite volcanoes generated in a post-collisional setting, associated with İBTZ area. Crater-shaped "calc-alkaline centers" have been intuitively recognized in previous publications, and have been drawn on geological maps (e.g. Agostini et al., 2010; Karaoğlu, 2014), although they miss a suitable volcanological description. The İBTZ zone was active during Early–Late Miocene when it generated a series of NE–SW elongated fluvio-lacustrine basins (Seyitoğlu et al., 1997; Aydar, 1998; Yılmaz et al., 2000; Uzel and Sözbilir, 2008; Ersoy et al., 2012a,b; Karaoğlu and Helvacı, 2012a,b; Uzel et al., 2013) associated with contemporaneous volcanic activity.

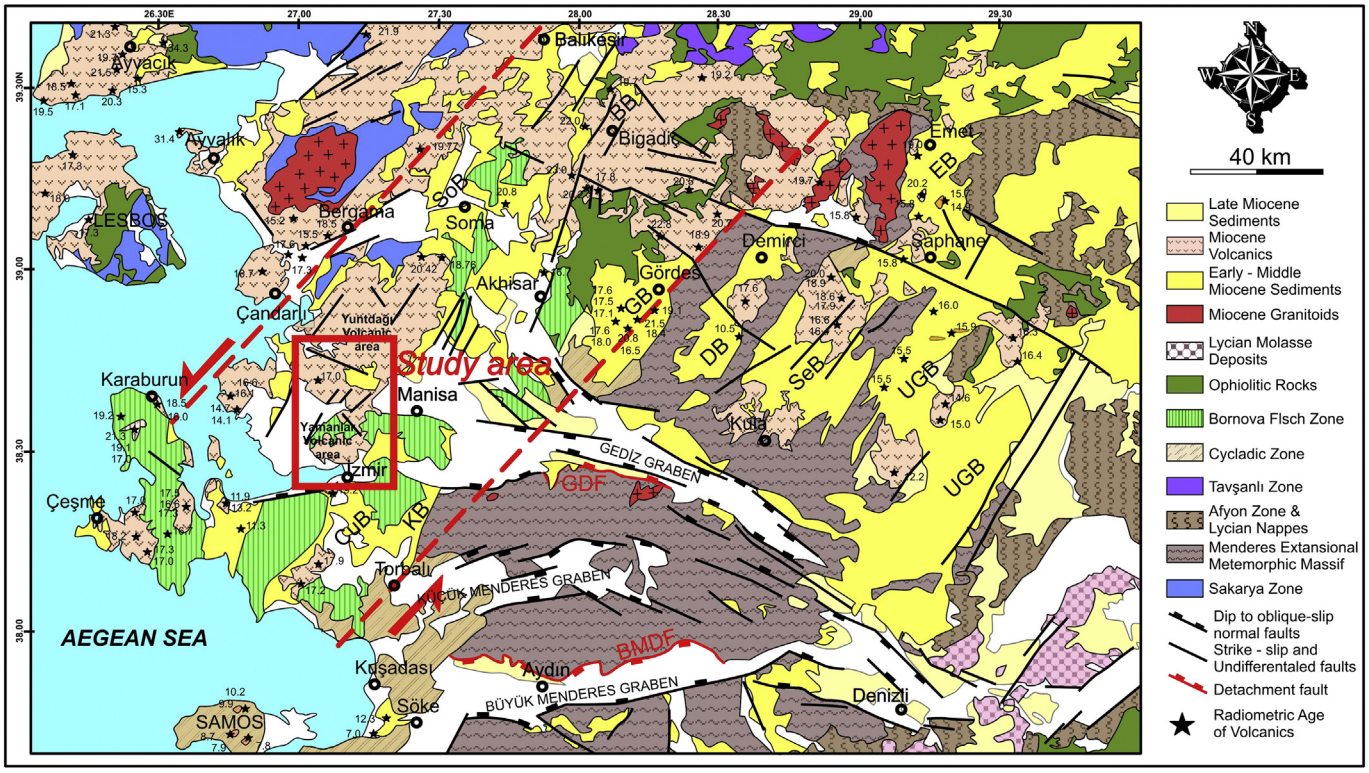

Fig. 2. Geological map of the western Anatolia showing the distribution of the Neogene basins, radiometric ages of the volcanic intercalations in the Neogene sediments and major structures and our study area (modified from 1/500 000 scaled geological map of Turkey (MTA); Abbreviations for granitoids: EyG: Eybek, KzG: Kozak, AG: Alaçamdağ, Kog, Koyunoba, EG: Eğrigöz, BG: Baklan, TG: Turgutlu and SG: Salihli granitoids. Abbreviations for basins: KB: Kocaçay Basin, BB: Bigadiç Basin; CuB: Cumaovası Basin; SoB: Soma Basin, GB: Gördes Basin, DB: Demirci Basin, SeB: Selendi Basin, UGB: Uşak–Güre Basin, EB: Emet Basin. Abbreviations for detachments: GDF: Gediz (Alaşehir) Detachment Fault, SDF: Simav Detachment Fault, BMDF: Büyük Menderes Detachment Fault (after Ersoy et al., 2014 with modifications).

The volcanic products consist of high-K calc-alkaline and minor K-alkaline and ultrapotassic rocks, suggested to derive from the lithospheric mantle and/or mixing with lower crustal melts (Borsi et al., 1972; Akay and Erdoğan, 2004; Erkül et al., 2005a,b; Innocenti et al., 2005; Agostini et al., 2010; Ersoy et al., 2010, 2012a,b; Chakrabarti et al., 2012).

This paper is based on volcanological field observations performed on several profiles crossing two volcanic areas, on K–Ar age determinations and geochemical analyses of representative samples. Here we discuss the eruptive history of the Yamanlar and Yuntdağı composite volcanoes, attempting to evaluate their generation in the post-collisional extensional geodynamic context.

2. Geologic setting

The pre-Miocene basement is characterized by the Bornova Flysch Zone (BFZ), (Erdoğan, 1990; Okay et al., 2012), known as an olistostrome–mélange belt, lying between the Menderes Metamorphic Core Complex and Sakarya zone, as part of the İzmir–Ankara Tethyan suture (Figs. 1, 2). It is composed of tectonized gravity mass flows, locally metamorphosed, of Late Cretaceous–Paleocene age, with blocks of Mesozoic limestones, serpentinites and submarine ophiolitic mafic volcanic rocks. The formation of the BFZ coincides with the Cretaceous subduction and HP/LT metamorphism of the northern passive continental margin of the Anatolide–Tauride Block (Okay et al., 2012).

The area was active during the Early Miocene extension, when various deposits unconformably cover the BFZ. The Early–Middle Miocene deposits of the studied area consist of two sedimentary units overlain by the Yamanlar volcanics (acc. to Uzel et al., 2013), or Yuntdağı volcanic unit (acc. to Özkaymak et al., 2013), i.e. the Kızıldere formation, consisting of conglomerates at the base grading upwards into sandstone-shale alternations and the Sabuncubeli formation, consisting of mudstones and then limestones. The sedimentary rocks pass into volcanic deposits. Late Miocene sediments are also known along İBTZ area, sometimes associated with basaltic volcanic rocks (e.g. Ersoy et al., 2014).

3. Methods

3.1. Geochemistry

Rock powders of the selected fresh rock samples were prepared by removing the altered surfaces and powdered in a shatter box at Dokuz Eylül University. The geochemical data for 17 samples were performed by ACME Analytical Laboratories Ltd. in Vancouver (Table 1). Element abundances were determined by ICP–AES (major elements) and ICP–MS (trace elements), following a lithium metaborate–tetraborate fusion and dilute nitric acid digestion of a 0.1 g sample. Weight Loss on ignition (LOI) was determined by weight difference after ignition at 1000 °C. The precision for major elements was less than 1%. The precision for trace elements was in the order of 10% relative.

3.2. K–Ar dating methodology

The K–Ar measurements obtained at the K–Ar laboratory of the Institute for Nuclear Research, Debrecen Hungary used the following methodology: After the fifteen rock samples were optically examined, about 1 kg of each sample was broken into small pieces free of weathering, xenoliths and joints. These whole-rock pieces were retained, crushed and sieved to 150–300 μm size fraction using copper sieves. The fine powder was elutriated with distilled water and oven dried at

Table 1
Whole-rock major and trace element analyses of representative samples from Yamanlar and Yuntdağı volcanoes.

Sample	52	52A	53	54	55	55A	56	57	59	60	61	62	65	67	68	69	70
Volcanic form	Lava	Dyke	Dyke	Dyke	Lava	Lava	Lava	Lava	Lava	Lava	Dyke	Intrusion	Lava	Lava	Lava	Lava	Lava
SiO_2	55.46	59.75	59.84	61.40	57.46	59.18	59.04	59.69	56.76	57.67	59.17	57.52	59.78	61.64	60.04	68.66	54.77
Al_2O_3	15.50	16.44	15.23	15.56	14.96	16.15	16.88	14.90	17.40	16.73	15.54	16.17	16.82	16.42	16.64	15.04	17.32
Fe_2O_3	6.11	5.51	5.32	4.79	5.46	5.32	6.15	6.01	7.40	6.39	5.62	5.91	5.33	5.03	5.50	3.14	5.86
MgO	2.81	2.74	2.77	2.10	2.98	2.19	2.94	3.17	2.73	2.95	1.99	2.81	2.90	2.46	3.13	0.26	2.52
CaO	6.51	4.52	4.38	3.76	6.97	4.75	6.04	5.38	6.82	6.06	4.05	6.11	5.13	4.99	5.43	1.60	7.52
Na_2O	2.78	3.54	3.03	2.75	2.50	3.18	3.13	2.89	3.12	2.93	2.56	2.54	3.33	3.31	3.42	3.47	2.99
K_2O	3.70	2.44	3.92	3.44	3.21	2.41	2.91	4.00	2.57	3.44	3.29	3.40	3.07	3.20	3.16	5.31	3.49
TiO_2	0.77	0.60	0.64	0.53	0.64	0.58	0.75	0.74	0.81	0.84	0.55	0.79	0.68	0.62	0.69	0.38	0.99
P_2O_5	0.32	0.19	0.32	0.22	0.35	0.18	0.26	0.40	0.30	0.38	0.15	0.32	0.26	0.21	0.25	0.09	0.49
MnO	0.11	0.08	0.11	0.09	0.13	0.08	0.09	0.08	0.11	0.11	0.15	0.08	0.10	0.09	0.10	0.03	0.13
LOI	5.60	3.90	4.10	5.10	4.70	5.70	1.40	2.30	1.60	2.10	6.80	4.00	2.30	1.70	1.30	1.70	3.50
Total	99.64	99.70	99.64	99.71	99.36	99.72	99.65	99.60	99.66	99.62	99.81	99.61	99.69	99.73	99.68	99.68	99.54
Cs	6.0	1.3	2.6	5.1	4.0	1.9	3.3	5.0	3.1	6.3	19.4	2.1	4.2	6.5	5.9	15.9	5.9
Rb	163.1	62.4	141.7	127.1	110.7	69.5	104.8	155.3	92.3	149	139.1	118.7	117.2	124.5	120.8	250.7	134.4
Ba	1266	1044	1325	1073	1364	959	1063	1307	1174	1301	629	1,336	930	921	960	1234	1695
Sr	664.5	610.4	526.5	427.9	750.5	688.5	658.8	689.3	677.8	717.3	244.7	777.6	611.1	522.4	601.6	420	918
Pb	2.3	14.5	13.7	10	2.9	12.1	3.3	2.8	4.5	3.6	7.4	4.9	4.2	2.4	3.4	6.8	3.7
Th	29.80	15.20	17.30	16.60	17.70	15.10	15.30	23.80	13.90	23.40	13.60	31.20	23.50	21.40	21.20	49.20	19.70
U	6.8	4.2	4.8	4.6	5.3	3.7	4.1	6.5	3.5	5.7	4.1	7.6	6.6	5.8	5.9	10.4	4.9
Zr	222.7	138.4	177.8	172.3	179.9	146.3	189.0	261.6	165.9	211.2	153.7	241.0	163.8	171.3	175.5	451.5	215.3
Hf	5.8	3.6	6.1	4.8	5.6	4.5	5.0	7.3	5.1	5.8	4.9	7.4	4.4	5.2	4.3	12.7	6.2
Ta	0.8	0.7	0.9	0.7	0.8	0.8	0.7	1.2	0.6	0.7	0.6	1.0	0.7	0.7	1.0	1.5	0.7
Y	20.5	23.9	24.3	22.6	21.5	22.9	26.9	27.4	24.7	23.2	21.6	22.0	19.4	19.2	24.0	21.5	22.1
Nb	14.4	10.2	13.7	11.1	11.6	9.9	10.6	15.6	9.0	12.5	9.7	14.9	11.7	11.6	13.4	25.0	13.5
Sc	15	13	14	11	17	12	18	17	19	18	12	15	13	12	13	6	18
Ni	13.8	6.2	67.9	21.3	49.2	4.3	8.9	168.8	7.3	9.7	4.9	13.7	10.9	12.0	28.0	1.4	19.2
Co	19.1	18.8	52.5	33.1	48.1	21.4	44.9	52.9	30.4	30.5	11.7	27.4	35.3	23.9	30.3	28.2	43.5
V	139	90	95	85	131	79	157	125	176	160	94	136	107	95	118	10	181
W	23.7	50.9	304.6	195.3	248.7	73.7	218.7	235.6	78.3	88.2	42.6	99.5	127.1	87.3	107.9	217.8	191.2
Ga	17.6	17.6	16.7	16.9	17.1	17.4	18.6	16.9	18.9	18.8	17.8	17.9	17.7	16.8	17.9	16.3	19.8
Zn	46	60	55	53	45	50	40	44	51	44	49	59	34	46	41	46	56
Cu	31.5	14.9	18.0	12.8	29.5	10.6	22.2	30.2	24.3	38.4	10.3	28.5	20.7	19.9	31.3	5.8	31.1
La	48.1	36.8	37.9	36.9	40.2	39.1	40.8	51.7	37.5	43.4	32.4	51.0	52.2	40.7	46.7	83.6	47.8
Ce	91.5	70.8	70.8	67.0	78.0	73.2	75.5	92.2	71.0	84.2	61.9	93.6	92.9	75.5	82.1	127.8	92.8
Pr	9.53	7.51	7.99	7.31	8.55	7.79	8.69	11.62	7.95	9.32	6.51	9.90	9.58	7.69	8.63	14.17	10.08
Nd	37.1	28.8	28.4	27.5	29.4	30.0	35.5	44.9	29.6	35.6	23.3	34.8	33.5	25.3	29.1	47.9	36.7
Sm	6.22	5.25	5.76	5.38	5.72	5.65	6.16	7.83	6.07	6.19	4.48	5.90	5.46	4.77	5.21	7.46	6.48
Eu	1.36	1.14	1.23	1.17	1.23	1.19	1.42	1.54	1.43	1.42	0.97	1.33	1.34	1.10	1.28	1.47	1.53
Gd	4.86	4.43	4.89	4.29	4.59	4.52	5.13	5.95	5.18	5.15	4.10	4.73	4.44	4.07	4.71	5.28	5.32
Tb	0.71	0.74	0.76	0.69	0.71	0.70	0.83	0.93	0.80	0.79	0.64	0.73	0.66	0.61	0.69	0.77	0.81
Dy	3.82	3.74	3.57	3.8	3.79	3.57	4.4	4.43	4.46	4.45	3.67	4.22	3.29	3.11	3.66	3.95	3.78
Ho	0.77	0.85	0.89	0.79	0.83	0.85	0.95	1.00	0.90	0.80	0.72	0.74	0.73	0.63	0.80	0.80	0.80
Er	2.04	2.35	2.33	2.28	2.04	2.27	2.58	2.89	2.67	2.26	2.13	2.16	2.24	1.95	2.33	2.46	2.37
Tm	0.36	0.37	0.42	0.37	0.37	0.40	0.43	0.45	0.40	0.35	0.35	0.35	0.34	0.30	0.33	0.41	0.39
Yb	2.13	2.61	2.58	2.38	2.27	2.41	2.64	2.65	2.48	2.33	2.39	2.26	2.02	2.21	2.15	2.59	2.11
Lu	0.36	0.35	0.41	0.35	0.37	0.38	0.40	0.40	0.40	0.38	0.34	0.33	0.32	0.30	0.37	0.40	0.30

110 °C for 24 h. One portion of the ready-made whole-rock sample was grounded in agate mortar for potassium analyses carried out with flame photometry.

Details of the analytical methods have been reported by Balogh (1985), Pécskay et al. (2006) and Odin et al. (1982). K–Ar ages were calculated using decay constants suggested by Steiger and Jäger

Table 2
K/Ar data of representative samples from Yamanlar and Yuntdağı volcanoes.

Nr. crt.	No. of K/Ar	Sample name	Rock type	K (%)	$^{40}Ar_{rad}$ (ccSTP/g) × 10^{-6}	$^{40}Ar_{rad}$ (%)	K/Ar age (Ma)	Volcanic area
1	8207	052	Andesite lava	2.404	1.5561	19.9	16.57 ± 1.16	Yamanlar
2	8208	052A	Andesite dyke	1.772	1.1738	54.8	16.96 ± 0.58	Yamanlar
3	8209	053	Andesite dyke	3.184	1.8573	42.9	14.94 ± 0.58	Yamanlar
4	8210	054	Dacite dyke	2.463	1.6816	32.9	17.48 ± 0.80	Yamanlar
5	8211	056	Andesite dome lava	2.039	1.2509	11.2	15.71 ± 1.94	Yamanlar
6	8212	057	Andesite dome lava	2.325	1.5972	83.0	17.58 ± 0.54	Yamanlar
7	8213	059	Andesite lava	2.057	1.2886	74.7	16.04 ± 0.50	Yamanlar
8	8214	060	Andesite lava	2.959	1.9958	46.9	17.27 ± 0.64	Yuntdağı
9	8215	061	Dacite intrusion	3.015	1.8687	35.5	15.87 ± 0.69	Yuntdağı
10	8216	062	Andesite intrusion	2.545	1.4921	11.6	15.02 ± 1.75	Yuntdağı
11	8217	065	Andesite lava	2.52	1.5533	46.0	15.79 ± 0.59	Yuntdağı
12	8218	067	Andesite lava	2.67	1.6579	42.6	15.90 ± 0.62	Yuntdağı
13	8219	068	Andesite lava	2.24	1.5065	43.0	17.22 ± 0.67	Yuntdağı
14	8220	069	Rhyolite lava	4.13	2.8270	44.2	17.52 ± 0.67	Yuntdağı
15	8221	070	Andesite clast in pyroclastic flow	2.78	1.8078	46.6	16.65 ± 0.62	Yuntdağı

(1977). The inter-laboratory standards Asia 1/65, LP-6, HD-B1 and GL-O, as well as atmospheric Ar were used to control the measurements. All analytical precision is reported at the 1σ level.

4. Volcanological observations

4.1. Structure of volcanic edifices

The highly eroded present edifice height is up to ~800 m. In both cases (Yamanlar and Yuntdağı) it can be remarked an eroded quasi-circular crater-like rim and a much deeply eroded central vent area that has 6–7 km in diameter (Fig. 1). The central vent areas are occupied by a shallow subvolcanic intrusion complex. The cone-building association is dominated by lava flows or lava domes where most of them are eroded. Toward the periphery, insignificant pyroclastic deposits have been found in Yuntdağı, due to erosion and burial in younger Miocene sedimentary deposits (Fig. 1). The most suitable term for such kind of complex structures dominated by lava flows are composite volcanoes (e.g. Davidson and de Silva, 2000). To illustrate the distribution of deposits relative to vent for discussed composite volcano we used the terminology of Davidson and de Silva (2000).

4.2. Main vent area

The central vent areas, in both cases have a similar circular shape ~3 km in diameter, suggesting former craters characterized by the

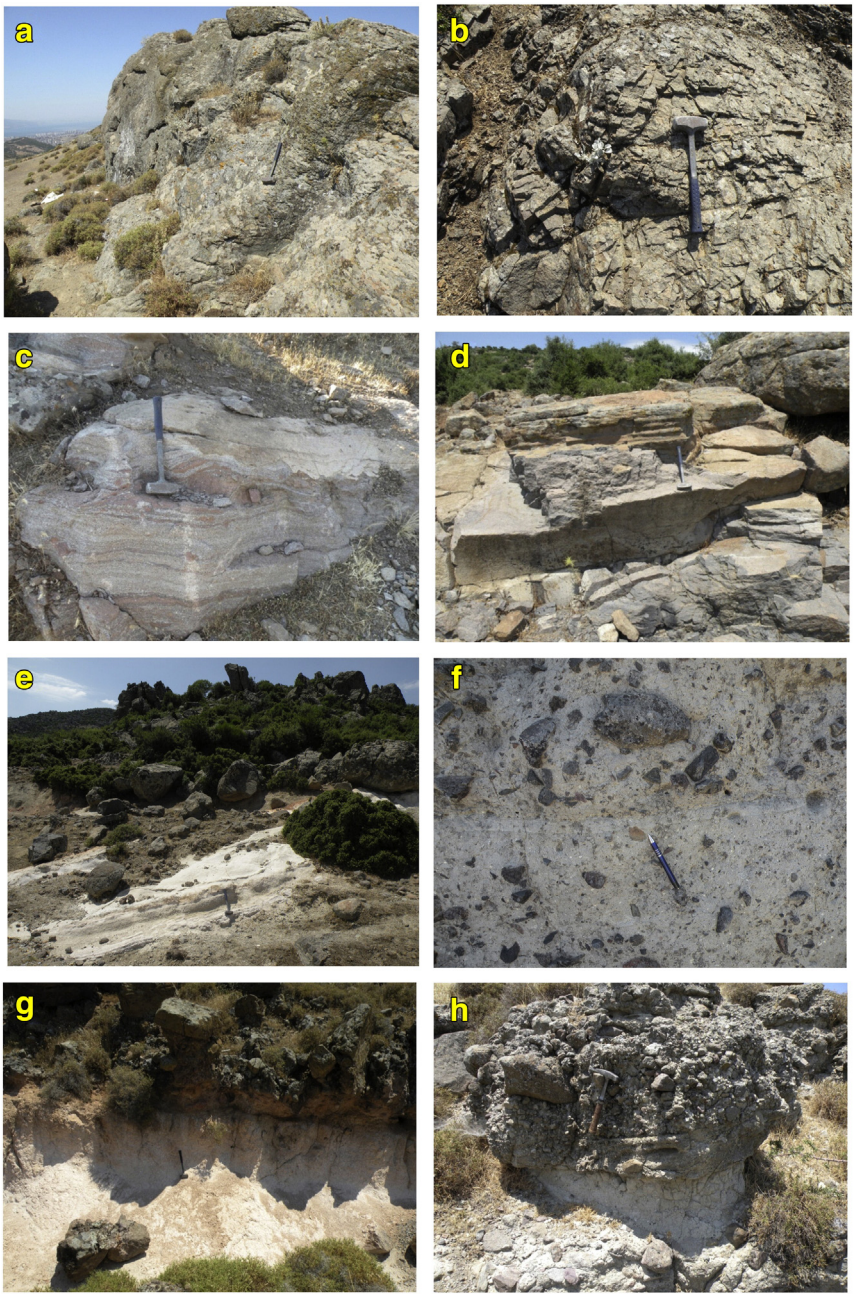

Fig. 3. a: 14.9 Ma eroded dyke in Yuntdağı intrusive feeding complex; b. 15.02 Ma irregular intrusive body (neck?) showing complex jointing in Yamanlar shallow subvolcanic intrusions; c. flow banding in Yamanlar lavas with inclusions of cognate inclusions; d. flow banding in lavas — Yuntdağı volcano; e. dominantly fall-out origin deposits intercalated in the lava dome flows in Yuntdağı volcano (see description in the text); f. pyroclastic block and ash flow deposits (see description in the text) in Yuntdağı volcano; g. Pyroclastic flow deposit (ignimbrite) in Yuntdağı volcano (see description in the text); h. sequence of fluvial conglomerates (showing cross-bedding at the base) in top of laharic (debris flow) deposits, characterized by heterolithic, various size, dominantly rounded and subrounded lithoclast, withish pumices, in a prevailing muddy–ashy matrix. The sequence represents part of ring-plain association around Yuntdağı volcano.

presence of numerous dykes (Figs. 1, 3a, b) or various-sized and irregularly shaped (neck-like) intrusions and lavas. The pervasive hydrothermal alteration of the subvolcanic intrusion complex is characteristic; propylitic alteration dominates over argillic as previously described in Yamanlar, with quartz veins associated with gold (Dora, 1964; Sayılı and Gonca, 1999).

4.3. Proximal cone association

Lava flows are the most common at the edges up to 1–2 km distance toward the exterior for both volcanoes and are characterized by a typical flow banding underlined sometimes by the structural variation given by difference in vesicularity. They are easily assigned to the vent area due to the divergent dip trend of flow banding. Lava domes are also observed at the present-day edifice edges, though it is difficult to imagine the extent of their distribution because of the strong erosional processes (Fig. 4). Dome-shape morphology can be viewed on a profile crossing the margin of the Yuntdağı crater (Fig. 1). They are the result of a more viscous flow and are characterized by a more massive appearance, sometimes showing large sub-vertical polygonal jointing. Polygonal scattered blocks are occasionally exposed at the top of the edifices, suggesting former dome structure, presently eroded.

4.4. Cone-building association

It is placed 2–10 km from the vent and it is dominated by fluidal lava flows and rare lava domes, which diverge all around the cone, sometimes associated with volcaniclastic deposits that have been observed only in Yuntdağı volcano. Several volcaniclastic lithologies have been detected:

4.4.1. Block and ash flow deposits

A sequence of monolithic breccia with ash-size matrix containing whitish lapilli-size pumices (1–2 cm in diameter), scoria with uneven rounded margins (2–3 cm in diameter) and variable, high contents of angular lithoclasts, consisting of monolithic andesite from 1 cm to 1.5 m size (Figs. 1, 3f). The sequence consists of several units of massive faintly bedded deposits of variable thickness (0.5–2 m), covering the eastern slopes of the Yuntdağı volcano and is intercalated in lava flows. The various beds are dominated by angular monolithic lithoclasts and are unsorted (Fig. 3f), main differences between the units consisting in the size and volume of the angular lithoclasts.

The features are typical for a sequence of pyroclastic block and ash flow deposits that succeeded at short time intervals.

4.4.2. Fall-out deposits

A volcaniclastic bedded sequence of whitish color and ~1.5–2 m thickness is intercalated between dome lava flows at point 066 (Fig. 3e). At its base it shows a 0.7 m sequence of cm-size beds consisting of various size, well sorted, ash to lapilli and angular-subangular massive andesite lithoclasts. In the upper part there is a discordant ashy-dominated layer, 0.8–1.4 m thick, showing a mixture of ashy material and rare lapilli-size lithoclasts.

In its lower part this sequence is characterized by several pulses of a fall-out origin that allowed the subaerial sorting processes. It resulted during the dome-forming processes. The upper discordant ashy massive layer could be a reworked material of the similar fall-out origin as the lower sequence.

4.4.3. Ignimbrites

At point 064 outcrops a ~3 m thick deposit showing large volumes of ashy matrix, reddish in color, with a rather homogeneous distribution of irregular pumice clasts that have various size (~5–20 cm), suggesting absence of grading. At the top, the last several cm show smaller size pumices (~1–2 cm) (Fig. 3g). It is covered discordantly by a blocky lava flow and overlays a different lava sequence.

The deposit is likely to represent a pyroclastic flow unit (ignimbrite) most probably emplaced in between lava- and dome generating events. The upper thin zone with smaller size pumices suggests to be reworked, as often the situation in non-welded ignimbrites.

4.5. Ring-plain association

This area is not well developed since it is presently buried under the surrounding much younger alluvial fans (Fig. 1). It locally surrounds the volcanoes and may not be considered part of the constructional edifice itself. Such deposits were observed at the southern margin of Yuntdağı (point 063 on Fig. 1). Here there is a sequence of interbedded fluvial conglomerates and lahar (debris flow) deposits (Fig. 3h), which form the distal edges of wedge-like fans of debris at the lower cone slopes.

5. Petrography and geochemistry

5.1. Petrography

5.1.1 . Yamanlar volcano

The analyzed samples are porphyritic, showing variable phenocryst load. However, there are some petrographic differences between volcanoes set by their main phenocryst phases. Plagioclase (andesine–bytownite, optically estimated), amphibole and biotite (13.5–18%, as

Fig. 4. a. Panorama of Yuntdağı eroded crater viewing from top toward the SW margins; note the erosional dome-shape aspect of an intrusive body inside the crater (photo courtesy by Ergin Umut Sayıl); b. panorama of Yamanlar eroded crater viewed from top-middle edge toward the SW. Note the remnant blocks of former dome structure in the foreground and rounded shape of present eroded margin of the crater.

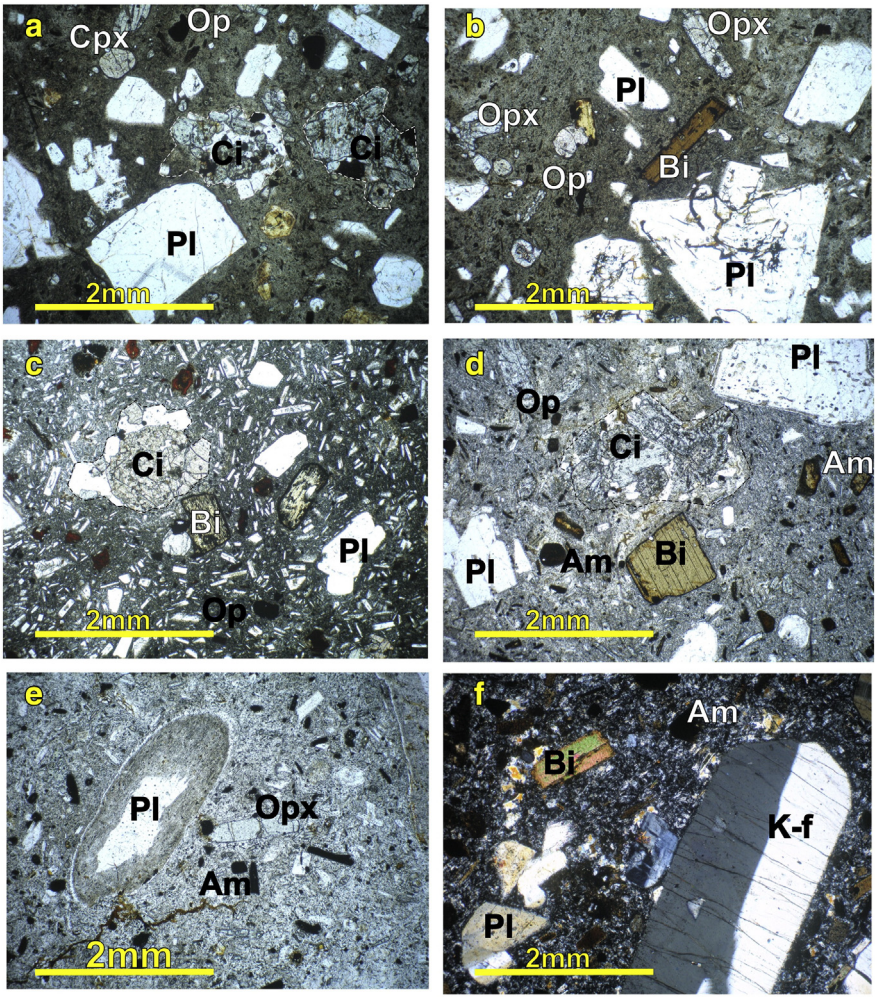

Fig. 5. Microscope view of selected samples (detailed description in Appendix 1). Location: Yamanlar volcano: a. sample 053, andesite dyke, note the rounded margins of plagioclase and irregular shape of cognate inclusions; b. sample 054, dacite dyke, note the presence of rounded margins of plagioclase and opacite around biotite; c. sample 059, andesite lava, note the presence of rounded margins of plagioclase, opacite around biotite and irregular shape of cognate inclusions; Yuntdağı volcano: d. sample 060, andesite lava, note the slight rounded margins of plagioclase, opacite around biotite and amphibole and irregular shape of cognate inclusion; e. sample 065, andesite lava, note the sieved and marginally corroded plagioclase and resorbed and marginally opacite amphibole; f. sample 069, rhyolite lava, note the large crystal of K-feldspar, resorbed amphibole and fresh biotite. Abbreviations: Pl — plagioclase; K-f — potassium feldspar; Amph — amphibole; Bi — biotite; Cpx — clinopyroxene; Opx — orthopyroxene; Op — opaque minerals; Ci — cognate inclusions.

modal) are the main phenocryst of Yamanlar (Appendix 1). Plagioclase is rarely sieved, but mostly presents irregular margin. Pyroxenes (clinopyroxene and orthopyroxene) and corroded quartz, besides of the ubiquitous apatite, opaque minerals and sphene are the main accessory minerals. Cognate inclusions (hypidiomorphic quasi-equigranular aggregates of plagioclase, pyroxene, amphibole and opaque minerals) showing sharp contacts and rounded margins with host andesite and resorption of plagioclase and opacite rims around biotite are frequent physiognomies (Fig. 5, Appendix 1). The size of cognate inclusions ranges in diameter from less than 0.5 cm to at least 20 cm, with median diameters less than 10 cm. They show rounded, spherical to lobate shapes and suggest to be genetically related to the host rocks.

5.1.2 . Yuntdağı volcano

Plagioclase (andesine–bytownite, optically estimated), pyroxenes (clinopyroxene and orthopyroxene), amphibole and biotite (up to 24%, as modal) are the main phenocryst phases in Yuntdağı (Appendix 1). Rare K-feldspar phenocrysts are present along plagioclase, amphibole and biotite in a single rhyolite sample (069), where the groundmass presents parallel uneven bands showing different types of glass devitrification, possibly suggesting flow banding. Cognate inclusions (aggregate of holocrystalline plagioclase, pyroxene and amphibole and opaque minerals) reach decametric size. Some of them show sharp contacts and rounded margins with host andesites, while others are characterized by some embayments. Other specific features of Yuntdağı are plagioclase sieve textures and/or irregular margins and biotite and amphibole marginal or total oxidation, and rare amphibole overgrowths on biotite (sample 067, Appendix 1).

5.2. Geochemistry

The LOI of the majority of the effusive rocks is about 1.3–2.3 wt.%. All the shallow subvolcanic intrusive rocks and a few lavas are variably affected by hydrothermal alteration. It was not possible to entirely avoid them and these samples display higher LOI (3.9–6.8 wt.%). This is the reason the results have been evaluated on an anhydrous basis in the classification and other diagrams.

On the total alkalis versus silica diagram (Fig. 6a) most samples plot within the sub-alkaline field at the limit with the latite field. According to Peccerillo and Taylor (1976) diagram (Fig. 6b) a large K_2O variation (2–4%) in a relatively large range of SiO_2 — 56–65% can be observed, with no evident correlation between K and silica. Most of the rocks fall randomly in the high-K andesite field, excepting three samples: two dacites (61, 54) and a rhyolite (69). Primitive mantle-normalized incompatible element patterns show negative anomalies for Nb–Ta, as well for P and Ti (Fig. 7a, b). There is a positive Pb anomaly that

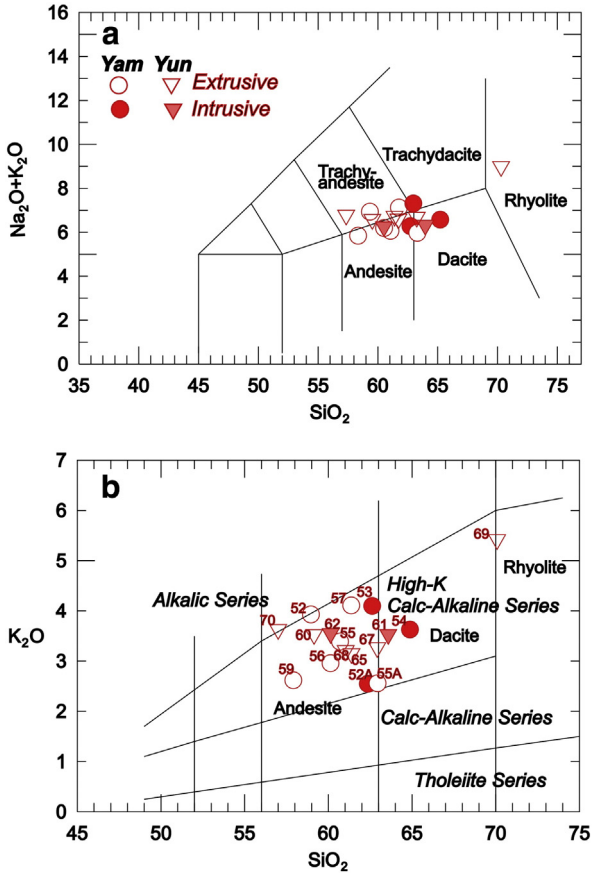

Fig. 6. a. Total alkali–silica (TAS) and b. K_2O–SiO_2 (Peccerillo and Taylor, 1976) diagrams for the studied rock samples. The sample labels reported in the Fig. 6a miss the initial zero.

characterizes mostly the intrusive rocks. The Chondrite CI-normalized REE patterns (Fig. 5c, d) show no essential differences between samples, all having a minor Eu negative anomaly ($Eu/Eu^* = 0.67–0.81$) and increased LREE, highest for the evolved rhyolite (069).

6. Timing of the volcanism

Results of dating on individual samples may not always be indicative of the age of the rock that might be affected by younger processes, such as alteration, loss or incorporation of excess radiogenic argon, etc. Several ways have been used to eliminate possible errors in the age assignment of rocks. Beside we selected fresh samples our data set was not depend on single sample age determination. A consistent set of results, in this case fifteen, diminishes the possibility of error in the age assignment. Since we did not get significant controversial results it was not necessary to date various gravity and magnetic fractions of the samples and construct isochrons to eliminate the influence of radiogenic Argon loss or excess. Fifteen K–Ar age data (7 for Yamanlar and 8 for Yuntdağı) are presented here in order to reveal the picture of volcanic evolution during the formation of composite volcanoes (Table 2). Samples were collected from the central part of the volcanoes represented by intrusive rocks, from the lava flow or eroded dome structures located at the topographic edges of the former crater areas (Figs. 1, 4) and from cone-building lava flows. In one case, a pyroclastic flow deposits (block and ash flow) from several km outside the volcano was also sampled (see the sample site distribution in Fig. 1).

There are three ages with 1σ precision higher than 1 Ma (two belongs to Yamanlar and one to Yuntdağı) however these ages fall in the interval of volcanic activity (Table 2), suggesting that they are meaningful and worth to be taken into consideration. The greater random analytical error should be in connection with the secondary alteration processes, however, the hydrothermal activity did not affect significantly the apparent ages. Thus these ages have also geological meaning and the random analytical error can be overestimated. The age interval of volcanic activity in both edifices spans for ~2.5 Ma, between 17.52–14.94 Ma with an average of 0.82 Ma 1σ precision range if we consider all the measurements, or 0.62 if we take out the analytical errors greater than 1, suggesting similar time length for both of them (Fig. 8). There is only one known age determination in our study area (S-906, yielding 17.0 ± 0.3 Ma, Rb–Sr age) of Ercan et al. (1996); however its exact location is only guessed (Fig. 2). Our data falls in the intervals reported by previous published data in the surrounding area (Borsi et al., 1972; Savaşçın, 1978; Ercan et al., 1996; Agostini et al., 2010; Ersoy et al., 2014) corresponding to Early–Middle Miocene, and they indicate the relative time between the inception and vanning of the volcanic activity in Yamanlar and Yuntdağı volcanoes.

It is to note that the most evolved rock, rhyolite (69), is also one of the oldest (17.52 ± 0.67 Ma). The youngest dated rocks (14.94 ± 0.58 Ma; 15.02 ± 1.75 Ma) are represented, in both cases, by intrusive rocks inside the shallow subvolcanic area inside the craters.

7. Discussion

7.1. Volcanic evolution

The K–Ar age determinations along volcanological observations are essential in understanding the comparative volcanic evolution of the volcanoes. The initial stages of volcanic activity were dominantly effusive and subaerial. Both volcanoes show a well-exposed shallow intrusive complex that in the case of Yamanlar exposes a large range of ages for the various intrusive bodies (17.48 ± 0.80 Ma; 16.96 ± 0.58 Ma; 14.94 ± 0.58 Ma), suggestive of a continuous activity connected to the vent area. The interval of volcanic activity is similar for both volcanoes (Fig. 8). The rhyolite lava exposed at ~4 km from the eastern border of Yuntdağı volcano represents one of the initial eruptions (17.52 ± 0.67 Ma). It is to note the contemporaneous activity in both edifices and the fact that the youngest dated rocks (14.94 ± 0.58 Ma; 15.02 ± 1.75 Ma) are represented, in both cases, by intrusive rocks inside the crater area. They represent the upper feeding system, and their presence at the surface suggests intensive erosion mostly facilitated by the pervasive hydrothermal alteration of some of it.

The erosion is mainly visible on the lavas and domes near the crater border. Differential erosion of the craters, opened and strongly eroded toward the SW resulted via block faulting along a NW–SE system and enhanced erosion due to an initial lower and larger fan-like alluvial drainage system inside the craters (e.g. Schumm et al., 2000; Fielitz and Seghedi, 2005; Tibaldi et al., 2006). If we take into account a missing age interval of ca. 0.7 ± 0.62 Ma from the youngest intrusive in the crater area up to the first dated lava flows of the proximal cone association (15.71 ± 1.94 Ma in Yamanlar and 15.79 ± 0.59 Ma in Yuntdağı) that is larger than assumed main repose-time of ~40 ka between supposed eruptions (Fig. 8), this may be susceptible to represent already eroded effusive part at the top edifices. Since the K–Ar ages argue to a rather continuous volcanic activity (Fig. 8), it may be suggested that magma output volume resulted from a constant number of active periods in each volcanoes history, separated by repose-time intervals that could be in the order of ~40^5 years.

7.2. Petrogenetic considerations

Recent studies indicate that Early–Middle Miocene medium- to high-K series andesites to rhyolites volcanic rocks along the strike-slip dominated the İzmir–Balıkesir Transfer Zone that include our study area, were most probably derived from mixing between mantle-derived magmas and lower crustal melts and formed the main source of the most primitive medium- to high-K andesitic rocks. Subsequent

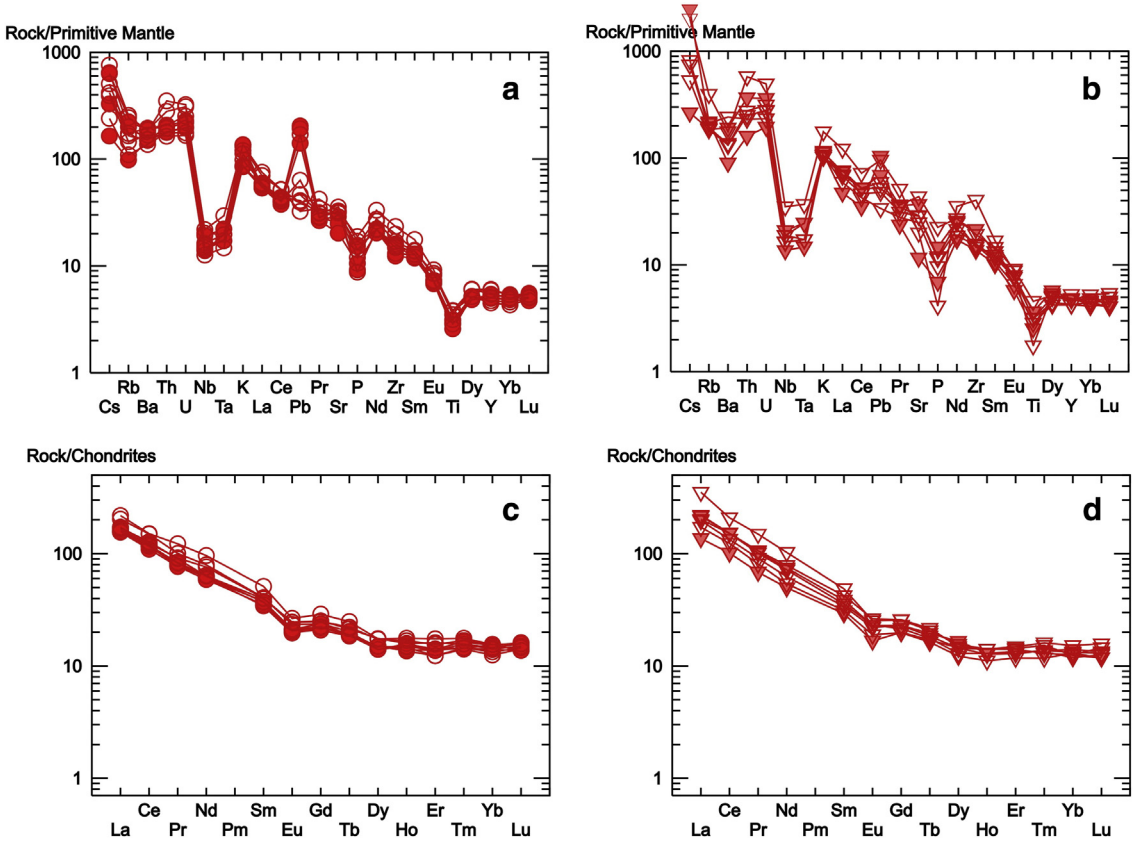

Fig. 7. a and b: Primitive Mantle (PM)-normalized and c and d: CI-chondrite normalized REE diagrams for Yamanlar and Yuntdağı volcanoes. Normalizing factors are from Sun and McDonough (1989). Symbols as in Fig. 6.

fractional crystallization (FC) and/or assimilation-fractional crystallization (AFC) processes that occurred are responsible for the wide range of chemical and petrographic types (Ersoy et al., 2012a; Ersoy and Palmer, 2013).

Our new geochemical data are in agreement with this hypothesis and we will attempt to demonstrate this. From a geochemical point of view, all the rocks are evolved, showing in the spider diagram/primitive mantle a negative anomaly for P and Ti that may characterize for partial melting (PM) of metasomatic mantle sources or fractional crystallization processes (FC) (Fig. 7a, b), with or without crustal contamination. Isotope data from the study areas confirm the implication of crustal assimilation (e.g. Agostini et al., 2010; Ersoy et al., 2012a). FC and/or PM is also suggested by high LREE/HREE (Fig. 7c, d) and a small negative Eu anomaly which likely infers plagioclase fractionation, typical for an upper crust magma storage system. The similar Eu anomaly of the rhyolite (069) suggest similar source as for andesites and important fractionation processes and relates them to "wet type cold-oxidized rhyolites" that may derive from a subduction-derived metasomatized mantle source (e.g., Bachmann and Bergantz, 2008).

To demonstrate the role of FC processes in Yamanlar and Yuntdağı volcanoes we made further group of Harker diagrams (Fig. 9). Increase in MgO, for the rocks with $SiO_2 < 62$, and absence of Ni depletion with respect to increasing SiO_2, suggest that olivine was not involved in the fractionating phases. Broad decrease in Ba coupled with decreasing MgO for the rocks with $SiO_2 > 62\%$ may be explained by fractionation of Mg and K-bearing phase such as biotite or amphibole. In this case, lateral variation (or even slightly decreasing) in Nb is not compatible with amphibole fractionation. Furthermore, the highly fractionated (high-SiO_2) rhyolite sample has the highest Nb content, refusing the amphibole fractionation. Therefore, decreasing MgO contents of the rocks with $SiO_2 > 62\%$ can be explained by biotite fractionation. A decrease in CaO/Al_2O_3 ratio coupled with decreasing V, Sc, CaO and TiO_2 contents may be indicative of extensive fractionation of clinopyroxene, but increasing the MgO up to $SiO_2 < 62\%$ may be used to refuse this interpretation. In this case, a decrease in Fe_2O_3 and TiO_2, V and Sc may be linked to Fe–Ti oxide fractionation. Extensive plagioclase fractionation is clearly evidenced by decreasing CaO, Sr, Eu, and Eu/Eu*. CaO depletion (and decrease in CaO/Al_2O_3) can also be link to plagioclase + apatite fractionation, instead of removal of clinopyroxene. Small degree apatite fractionation is also supported by the decreasing in REEs, especially in LREE, such as Ce. These observations led us to conclude that the fractionating assemblage responsible for the differentiation of the Yamanlar and Yuntdağı volcanics can be taken as plagioclase + biotite + Fe–Ti-oxides + apatite. Additionally, small amounts of clinopyroxene may also be included.

By using an assemblage of plagioclase (70%) + biotite (13%) + clinopyroxene (5%) + magnetite (5%) + apatite (5%), Sr/V vs. V systematics of the volcanic rocks have been modeled to test the validity of the fractional crystallization processes. In Fig. 10, the PETROMODELER program (Ersoy, 2013) is used with the increments of 10% and the partition coefficients compiled from GERM partition Coefficient data base (www.http://earthref.org/). The results show that the andesitic rocks may have been produced by 0–30% fractional crystallization of the most primitive sample (sample 70 with lowest silica content). The rhyolitic sample (69), on the other hand, require up to 80% fractionation. It is also to note that crustal contamination and mixing processes may have operated during this fractionation, but it is not possible to monitor this effect, since there are no available isotopic data from these samples.

Ratios of high field strength elements (HFSE) such as Nb and Zr can provide insight into variations in magma source composition (e.g. Davidson, 1996; Singer et al., 1996). Nb and Zr are depleted in subduction-related magmas and are assumed to be dominantly mantle-derived, being relatively immobile under hydrothermal

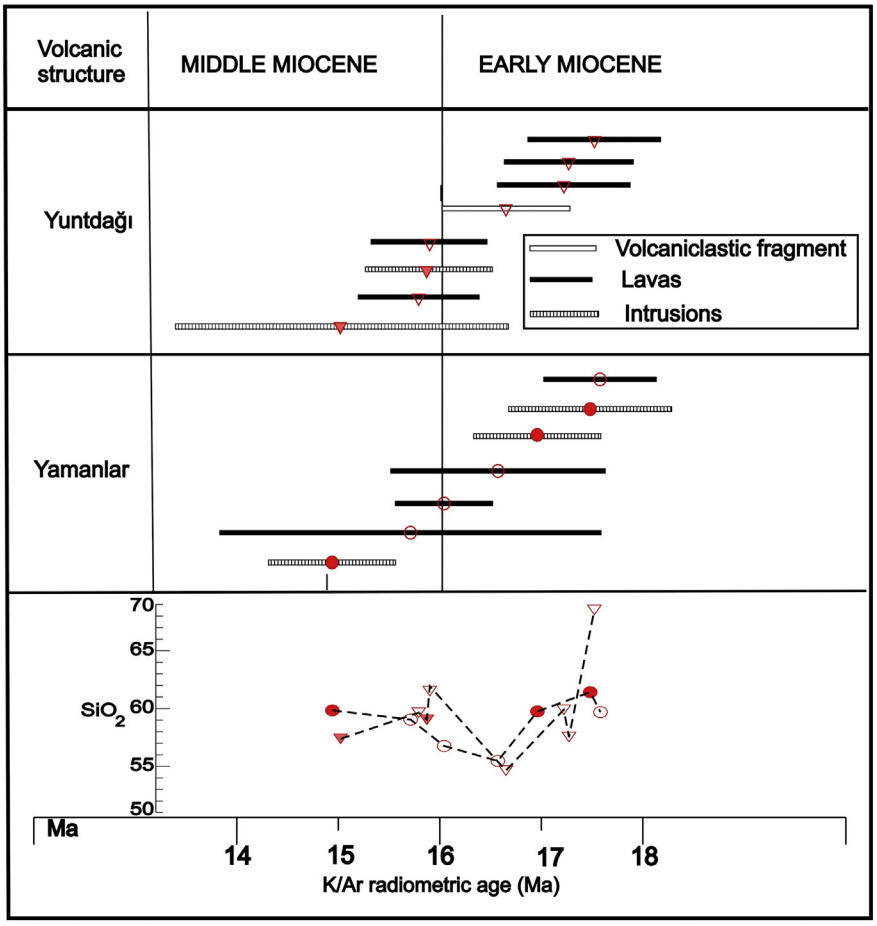

Fig. 8. Diagram of K/Ar ages with analytical errors and SiO_2 vs K/Ar ages in Yamanlar and Yuntdağı volcanoes. Symbols as in Fig. 6.

conditions and strongly fractionated only during melting or magma-mixing processes (Thirlwall et al., 1994; Davidson, 1996). Different Nb/Zr ratios are generally interpreted in terms of variations in source composition or changes in degree of partial melting of the mantle, since linear trends of Nb enrichment suggest fractional crystallization (e.g. Davidson, 1996). The Nb/Zr–Nb diagram for most primitive rock (~56 wt.% SiO2) (Fig. 11) shows Zr–Nb values starting from ~0.6–0.7, not far from a typical MORB value, but closer to the Lower and Middle Crust average values (Rudnick and Fountain, 1995). The plots follow both linear trends, starting from the most primitive rocks found in Yamanlar and Yuntdağı, in a small range along the mantle source composition or changes in degree of partial melting trend and mostly developed along the horizontal trend toward more differentiated rocks suggesting fractional crystallization, having at the end of the range the solitary rhyolite sample (69), with higher Nb contents.

These observations are in agreement with fractional crystallization modeling (Fig. 10). Another important observation is that the rhyolite sample (Yuntdağı) by showing similar Nb/Zr trend as the most primitive rock in the studied area is older (17.52 ± 0.67 Ma) than the other rocks in Yuntdağı, but has similar age with andesites of Yamanlar volcano. This may suggest that the rhyolite could derive via fractional crystallization processes from the similar source as other andesites, not from a different one. Without isotope data is difficult to say that the source, as suggested also by Fig. 11, is a slightly enriched mantle source or lower crust, or about the influence of assimilation processes, however, as already mentioned, the published data with isotopes in the surrounding areas are suggesting that both mantle and crustal melts are implicated in generation of these magmas (e.g. Agostini et al., 2010; Ersoy et al., 2012a), so most probably the source area is situated at the mantle–crust boundary.

Nevertheless, there are some additional petrogenetic considerations that derive from a combined petrographic and geochemical study in both volcanoes. Some textural characteristics of plagioclase, amphibole and biotite can give constraints on additional magma chamber processes.

The common presence of irregular and rounded margins which are observed for a large number of plagioclase crystals, beside combination with sieve textures (Fig. 5, samples 053, 054 and 060) points to marginal melting of these crystals and consequently a process of disequilibrium (in this case thermal (e.g. Nelson and Montana, 1992). This may indicate an influx of hotter magma inflow into a shallow, partially evolved magma storage system that implies mixing. The plagioclases with irregular and rounded margins indicate that re-equilibrium was not reached, suggesting that eruption occurred soon after mixing. The mass breakdown oxidation of amphiboles is also a sign of thermodynamic disequilibrium, which may be related to the increase in oxygen fugacity with increasing temperature which favors dehydroxylation (Graham et al., 1984). Such features of increasing temperature can be most easily explained in terms of magma mixing (Fig. 5, sample 065). The reaction rims of amphiboles and biotites, on the other hand, suggest that H_2O is leaving the system due to lowering pressure.

In the Peccerillo and Taylor (1976) diagram, the scatter plot distribution showing large K_2O variation (2–4%) in a relatively large range of SiO_2 — 56–65% may also confirm the local upper crustal mixing processes (Fig. 6a). The decrease in SiO_2 at ~16.5 Ma (Fig. 8) for both volcanoes could be interpreted in terms of mixing of an andesitic magma with a least evolved basaltic andesite. Overall, the identification

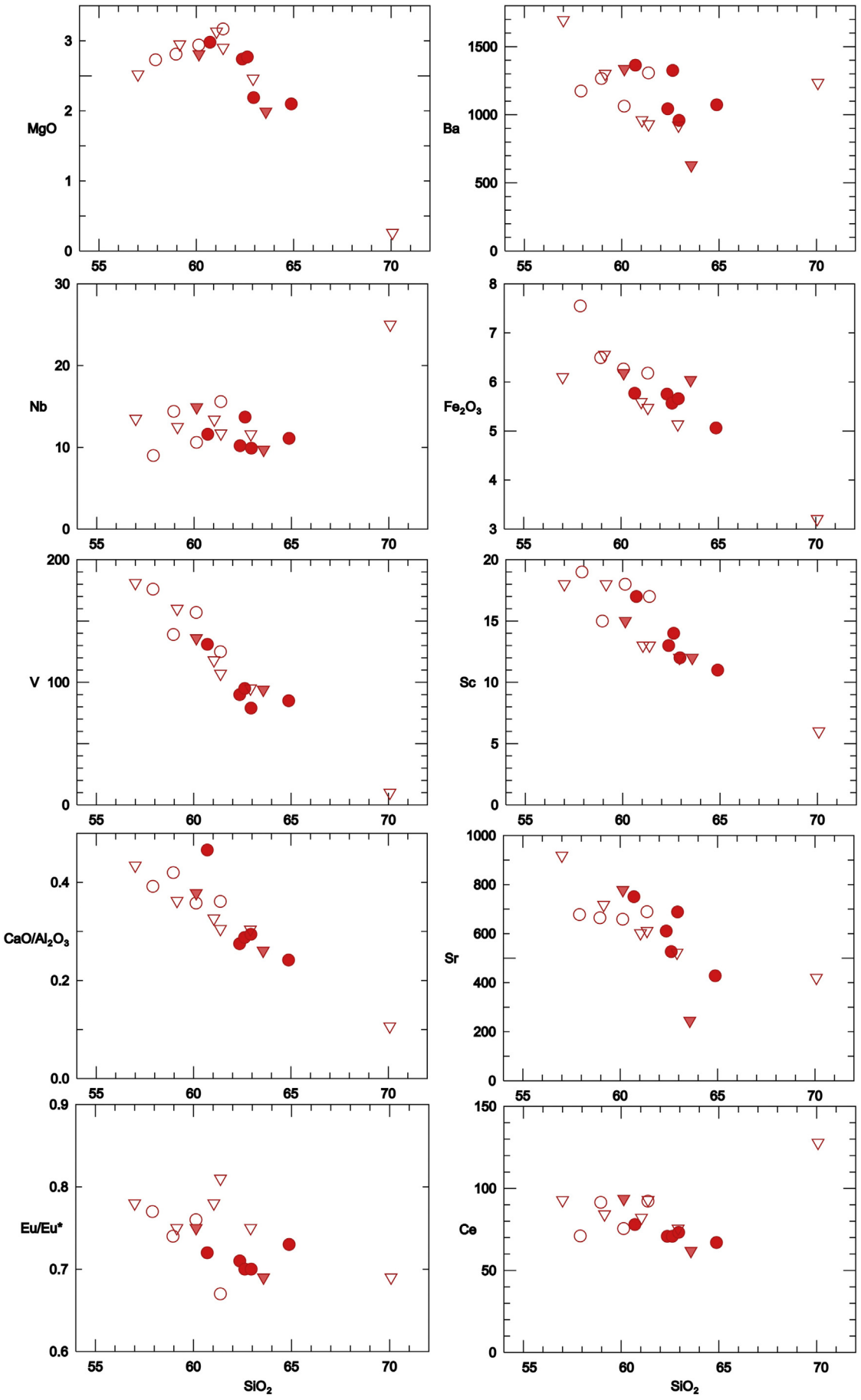

Fig. 9. Harker diagrams variations for selected elements and ratios. Symbols as in Fig. 6.

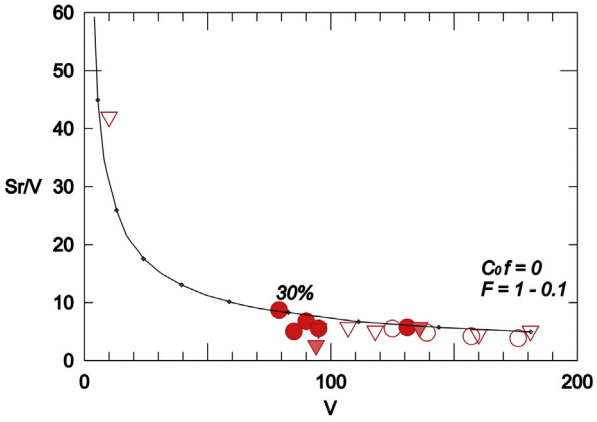

Fig. 10. Sr/V vs. V showing fractional crystallization modeling starting from the most primitive rock (70) of the Yamanlar and Yuntdağı rocks. Symbols as in Fig. 6.

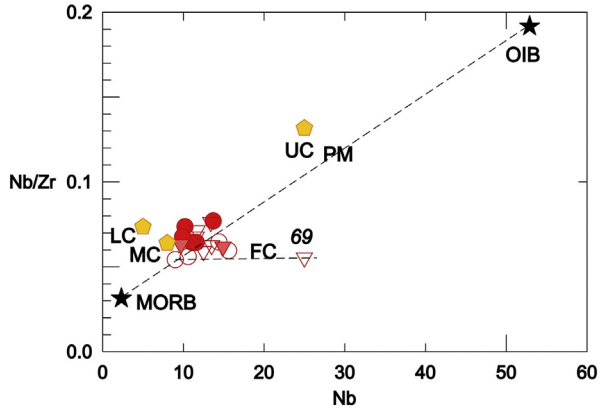

Fig. 11. Nb/Zr vs. Nb diagram for Yamanlar and Yuntdağı rocks. Symbols as in Fig. 6.

of mixing processes, even not always obvious by the geochemical features, suggest a very complex and dynamic magmatic system.

7.3. Geodynamic considerations

Tectonically, İBTZ is formed by NW–SE elongated volcano-sedimentary basins generated during Early–Middle Miocene that were further dissected by mainly NE–SW elongated Plio-Quaternary depressions. Miocene stratigraphy is typified by a folded tectonics. Normal and strike-slip faults are dissecting the volcano-sedimentary sequences, andesitic to rhyolitic volcaniclastic deposits and lava flows, and lacustrine deposits (Uzel et al, 2013).

In view of these general considerations, any tectonomagmatic model to infer magma generation must be able to explain the following observations:

1) The distribution of magmatic rocks is diffuse, covering a region of ~200 × 50 km along a NE–SW trend between south İzmir and Balıkesir. This area is only an apparent linear trend for various phases of magmatism that were closely connected to basin development. Besides, it has correspondent coeval magmatic products in basins associated to the Menderes Core Complex extensional evolution (e.g., Ersoy et al., 2010; Seghedi et al. 2013);
2) The magmatism post-dated the collision of the Sakarya continent and Anatolide–Taurides block, assembled during the late Cretaceous to Paleogene along the Vardar–İzmir–Ankara suture zone. The Late Cretaceous blueschist-facies rocks of the Tavşanlı Zone represents the subducted passive margin of the Anatolide–Taurides (Okay and Kelley, 1994; Sherlock et al., 1999);
3) The magma source was located in the upper mantle/lower crust area and the mantle was metasomatized by Late Cretaceous to Paleogene subduction.

Geochemical modeling of the Western Anatolia volcanic rocks demonstrates that the lithospheric mantle was extremely heterogeneous at the time of magma generation (e.g., Ersoy and Palmer, 2013). A heterogeneously enriched lithospheric mantle was the main source for the magmas produced during the first stages of extensional basin formation (e.g., Aldanmaz et al., 2000; Prelević et al., 2010; Ersoy et al., 2012a), and such source enrichment most probably belong to the last subduction event. Prelević et al. (2012) related the unusual mantle metasomatism of Western Anatolia volcanic rocks to the Late Cretaceous depletion event with generation of the supra-subduction magmas, by accepting a southern closure of the Neotethyan Ocean, its accretion under Tauride–Anatolide platform and then further metasomatic processes via tectonic imbrications with crustal material or sediments. Çoban et al. (2012) and Ersoy et al. (2012b) also suggested that contamination of the mantle source could be a result of the subduction of crustal slices during amalgamation processes of lithospheric blocks. The inferred metasomatic event was attributed to deep subduction involving crustal rocks during previous collisional events (e.g., Ersoy and Palmer, 2013) and before the inception of extensional processes.

Such geodynamic context was followed during Early–Middle Miocene by coeval core complex extension of the Menderes Massif and transtensional movements along İTBZ. We suggest that the triggering mechanism for magma generation along İTBZ, including Yamanlar and Yuntdağı volcanic fields, was decompression melting of upper lithospheric mantle/lower crust material during the Early–Middle Miocene regional transtensional movements. Similar triggering mechanism for magma generation was suggested for the Carpathian–Pannonian area during the similar time interval (Seghedi and Downes, 2011).

8. Conclusions

(1) We discuss with arguments the presence of two composite volcanoes (Yamanlar and Yuntdağı) along the southern edge of İBTZ. By attesting their relatively large, long-lived constructional volcanic edifice, dominated by lava flow and domes and less by volcaniclastic products erupted from one or more craterial-situated vents and proving the presence of their recycled equivalents in the cone-building and plain associations.
(2) Yamanlar and Yuntdağı volcanic fields represent complex composite volcanoes developed as subaerial in an extensional setting along İzmir–Balıkesir Transfer Zone at the crossing between NE–SW with NW–SE trending systems (e.g., Uzel et al, 2013: Ersoy et al., 2014).
(3) The crater diameters presently enlarged by erosion at ~6 km comprise various size intrusive forms, due to multiple feeding events that were accompanied by late-stage hydrothermal fluids. A proximal cone association with primary effusive material and cone-building association with dominant effusive and explosive products characterize both edifices.
(4) The volcanoes were developed between ~17.48–14.94 Ma. The ~2.5 Myr duration is longer than that of the average duration of the composite volcanoes in subduction-related systems, being appreciated to ~1 Myr (e.g. Davidson and de Silva, 2000). This range may eventually apply to other composite volcanoes generated in post-collisional extensional settings. We expect more such kind of edifices to be documented in the future along İzmir–Balıkesir Transfer Zone where the volcanic activity is showing similar age interval development (e.g. Ersoy et al., 2012b, 2014).
(5) The preservation of the typical cone morphology suggests that the erosion was not able to totally destroy their initial shape. Most likely, erosion was strongly influenced by strike-slip and

normal faulting tectonic activity associated with specific fluvial drainage that has differentially removed a thickness of ~500–1000 m during the last ~15 Myr, as suggested by similar situations in Apuseni Mts., in Carpathian–Pannonian Area (e.g., Seghedi et al. 2010; Merten et al., 2011). However, specific studies to understand the rate of erosion are necessary.

(6) Major and trace element contents along with petrographic data and geochemical modeling support the idea of initial fractional crystallization processes (associated with assimilation) followed by mixing processes in upper crustal chambers.

(7) An upper crustal-level co-genetic magma storage system allowing differentiation processes (FC, AFC) and mixing with magmas from deeper levels is also compatible with the extensional setting that may favor long-lived magma chamber processes (FC and assimilation), with exception of the oldest products (rhyolites) that suggests extended time for magma chamber FC (assimilation).

(8) Magma triggering mechanism is assumed to result via decompression melting of an upper mantle/lower crust source material during regional transtensional movements along İzmir–Balıkesir Transfer Zone in post-collisional setting;

(9) Further detailed volcanological, geochronological and geochemical studies are required to better quantify the volcanic evolution of the investigated area.

Supplementary data to this article can be found online at http://dx.doi.org/10.1016/j.jvolgeores.2014.12.019.

Acknowledgments

Analytical work of K/Ar dating was supported by, and performed within the framework of the academic bilateral cooperation agreement between the Institute of Geodynamics, Romanian Academy and the ATOMKI Debrecen, Hungarian Academy of Sciences. We benefited by a grant of the Ministry of National Education, CNCS–UEFISCDI, project number PN-II-ID-PCE-2012-4-0137. This work was also supported by the Dokuz Eylül University Scientific Project (Bilimsel Araştırma Projesi) No: 2010.KB.FEN.009. We thank Berk Çakmakoğlu and Yasin Aydın for their drafting assistance. We thank Yalçın Ersoy for his help with PETROMODELER geochemical program used for petrogenetic modeling. We recognize the assistance of Răzvan-Gabriel Popa, Çilem Karagöz, Mustafa Çetin, Özgür Karaoğlu and Bülent Kasapoğlu and Engin U. Sayıl during the laboratory and field studies. We thank Editor Joan Marti for his help and patience. Constructive comments provided by two anonymous reviewers helped us to clarify our views.

References

Agostini, S., Tokçaer, M., Savaşçın, M.Y., 2010. Volcanic rocks from Foça–Karaburun and Ayvalık–Lesvos Grabens (Western Anatolia) and their petrogenic–geodynamic significance. Turk. J. Earth Sci. 19, 157–184.

Akay, E., Erdoğan, B., 2004. Evolution of Neogene calc-alkaline to alkaline volcanism in the Aliağa-Foç a region (Western Anatolia, Turkey). J. Asian Earth Sci. 21, 367–387.

Aldanmaz, E., Pearce, J.A., Thirlwall, M.F., Mitchell, J.G., 2000. Petrogenetic evolution of late Cenozoic, post-collision volcanism in western Anatolia Turkey. J. Volcanol. Geotherm. Res. 102, 67–95.

Aydar, E., 1998. Early Miocene to Quaternary evolution of volcanism and the basin formation in western Anatolia: a review. J. Volcanol. Geotherm. Res. 85 (1), 69–82.

Bachmann, O., Bergantz, G.W., 2008. Rhyolites and their source mushes across tectonic settings. J. Petrol. 49, 2247–2285.

Balogh, K., 1985. K–Ar dating of Neogene volcanic activity in Hungary. Experimental technique, experiences and methods of chronological studies. ATOMKI Reports D/1, 277–288.

Borsi, S., Ferrara, G., Innocenti, F., Mazzuoli, R., 1972. Geochronology and petrology of recent volcanics in the eastern Aegean Sea (west Anatolia and Leovos Island). Bull. Volcanol. 36, 473–496.

Chakrabarti, R., Basu, A.R., Ghatak, A., 2012. Chemical geodynamics of Western Anatolia. Int. Geol. Rev. 54, 227–248.

Çoban, H., Karacık, Z., Ece, Ö.I., 2012. Source contamination and tectonomagmatic signals of overlapping Early to Middle Miocene orogenic magmas associated with shallow continental subduction and asthenospheric mantle flows in Western Anatolia: a record from Simav (Kütahya) region. Lithos 140–141, 119–141.

Davidson, J.P., 1996. Deciphering mantle and crustal signature in subduction zone magmatism. In: Bebout, G.E., Scholl, D.W., Kirby, S.H., Platt, J.P. (Eds.), Subduction Top to Bottom. Geophysical Monograph vol. 96, pp. 251–262.

Davidson, J., de Silva, S., 2000. Composite volcanoes. In: Sigurdsson, H., Houghton, B.F., McNutt, S.R., Rymer, H., Stix, J. (Eds.), Encyclopedia of Volcanoes. Academic Press, San Diego, pp. 665–681.

Dora, Ö., 1964. 1970, Arapdağ (Karşıyaka) kuvars-altın filonlarının mineralojik etüdü; Madencilik dergisi (in Turkish), cilt IX. Sayı 4, 25–41 (Mineralogic study of Arapdağ (Karşıyaka) quartz-gold veins. Mining Journal, IX, 4, 25-41).

Ercan, E., Satır, M., Sevin, D., Türkecan, A., 1996. Some new radiometric ages from Tertiary and Quaternary volcanic rocks from West Anatolia (in Turkish). Bull. Mineral Res. Explor. Inst. Turk. 119, 103–112.

Erdoğan, B., 1990. Tectonic relations between İzmir–Ankara Zone and Karaburun Belt. Bull. Mineral Res. Explor. Inst. Turk. 110, 1–15.

Erkül, S.T., 2012. Petrogenetic evolution of the Early Miocene Alaçamdağ volcano–plutonic complex, northwestern Turkey: implications for the geodynamic framework of the Aegean region. Int. J. Earth Sci. 101, 197–219.

Erkül, S.T., Erkül, F., 2012. Magma interaction processes in syn-extensional granitoids: the Tertiary Menderes Metamorphic Core Complex, western Turkey. Lithos 142–143, 16–33.

Erkül, F., Helvacı, C., Sözbilir, H., 2005a. Evidence for two episodes of volcanism in the Bigadic borate basin and tectonic implications for western Turkey. Geol. J. 40, 545–570.

Erkül, F., Helvacı, C., Sözbilir, H., 2005b. Stratigraphy and geochronology of the Early Miocene volcanic units in the Bigadiç borate basin, Western Turkey. Turk. J. Earth Sci. 14, 227–253.

Ersoy, E.Y., 2013. PETROMODELER (Petrological Modeler): a Microsoft ® Excel© spreadsheet program for modelling melting, mixing, crystallization and assimilation processes in magmatic systems. Turk. J. Earth Sci. 22, 115–125. http://dx.doi.org/10.3906/yer-1104-6 (© TÜBİTAK).

Ersoy, E.Y., Palmer, M.R., 2013. Eocene–Quaternary magmatic activity in the Aegean: implications for mantle metasomatism and magma genesis in an evolving orogeny. Lithos 180–181, 5–24.

Ersoy, E.Y., Helvacı, C., Palmer, M.R., 2010. Mantle source characteristics and melting models for the early middle Miocene mafic volcanism in Western Anatolia: implications for enrichment processes of mantle lithosphere and origin of K-rich volcanism in post-collisional settings. J. Volcanol. Geotherm. Res. 198, 112–128.

Ersoy, Y.E., Helvacı, C., Palmer, M.R., 2011. Stratigraphic, structural and geochemical features of the NE–SW trending Neogene volcano–sedimentary basins in western Anatolia: implications for associations of supra-detachment and transtensional strike-slip basin formation in extensional tectonic setting. J. Asian Earth Sci. 41, 159–183.

Ersoy, E.Y., Helvacı, C., Uysal, İ., Karaoğlu, Ö., Palmer, M.R., Dindi, F., 2012a. Petrogenesis of the Miocene Volcanism along the İzmir–Balıkesir Transfer Zone in western Anatolia, Turkey: implications for origin and evolution of potassic volcanism in post-collisional areas. J. Volcanol. Geotherm. Res. 241–242, 21–38.

Ersoy, E.Y., Helvacı, C., Palmer, M.R., 2012b. Petrogenesis of the Neogene volcanic units in the NE–SW-trending basins in western Anatolia, Turkey. Contrib. Mineral. Petrol. 163, 379–401.

Ersoy, E.Y., Çemen, İ., Helvacı, C., Billor, Z., 2014. Tectono-stratigraphy of the Neogene basins in Western Turkey: implications for tectonic evolution of the Aegean Extended Region. Tectonophysics http://dx.doi.org/10.1016/j.tecto. 2014.09.002.

Fielitz, W., Seghedi, I., 2005. Late Miocene–Quaternary volcanism, tectonics and drainage system evolution in the East Carpathians, Romania. Tectonophysics 410, 111–136.

Francis, P., 1993. Volcanoes, a Planetary Perspective. Oxford University Press, Oxford (443 pp.).

Göktaş, F., 2014. Neogene stratigraphy of the northern part of Karaburun Peninsula (in Turkish). MTA Derg. 148, 43–60.

Graham, C.M., Harmon, R.S., Sheppard, S.M.F., 1984. Experimental hydrogen isotope studies: hydrogen isotope exchange between amphibole and water. Am. Mineral. 69, 128–138.

Helvacı, C., Ersoy, Y., Sözbilir, H., Erkül, F., Sümer, Ö., Uzel, B., 2009. Geochemistry and $^{40}Ar/^{39}Ar$ geochronology of Miocene volcanic rocks from the Karaburun Peninsula: implications for amphibole-bearing lithospheric mantle source, Western Anatolia. J. Volcanol. Geotherm. Res. 185, 181–202.

Innocenti, F., Agostini, S., Di Vincenzo, G., Doglioni, C., Manetti, P., Savaşçın, M.Y., Tonarini, S., 2005. Neogene and Quaternary volcanism in Western Anatolia: magma sources and geodynamic evolution. Mar. Geol. 221, 397–421.

Karaoğlu, Ö., 2014. Tectonic controls on the Yamanlar volcano and Yuntdağı volcanic region, western Turkey: implications for an incremental deformation. J. Volcanol. Geotherm. Res. 274, 16–33.

Karaoğlu, Ö., Helvacı, C., 2012a. Growth, destruction and volcanic facies architecture of three volcanic centres in the Miocene Uşak–Güre basin, western Turkey: subaqueous–subaerial volcanism in a lacustrine setting. J. Volcanol. Geotherm. Res. 245–246, 1–20.

Karaoğlu, Ö., Helvacı, C., 2012b. Structural evolution of the Uşak–Güre-supra-detachment basin during Miocene extensional denudation in western Turkey. J. Geol. Soc. Lond. 169 (5), 627–642.

Kayseri-Özer, M.S., Sözbilir, H., Akgün, F., 2014. Miocene palynoflora of the Kocaçay and Cumaovası basins: a contribution to the synthesis of Miocene palynology, palaeoclimate, and palaeovegetation in western Turkey. Turk. J. Earth Sci. 23, 233–259.

Lexa, J., Seghedi, I., Németh, K., Szakács, A., Konečný, V., Pécskay, Z., Fülöp, A., Kovacs, M., 2010. Neogene–Quaternary volcanic forms in the Carpathian–Pannonian Region: a review. Cent. Eur. J. Geosci. 2 (3), 207–270.

Merten, S., Matenco, L., Foeken, J.P.T., Andriessen, P.A.M., 2011. Toward understanding the post-collisional evolution of an orogen influenced by convergence at adjacent plate margins: Late Cretaceous–Tertiary thermotectonic history of the Apuseni Mountains. Tectonics 30, TC6008.

Nelson, S.T., Montana, A., 1992. Sieve-textured plagioclase in volcanic rocks produced by rapid decompression. Am. Mineral. 77, 1242–1249.
Odin, S.S. (Ed.), 1982. Numerical Dating in Stratigraphy (Part I and Part II). John Willey and Sons, New York (1040 pp.).
Okay, A.I., Kelley, S.P., 1994. Tectonic setting, petrology and geochronology of jadeite + glaucophane and chloritoid + glaucophane schists from north-west Turkey. J. Metamorph. Petrol. 12, 455–466.
Okay, A.I., Işıntek, İ., Altıner, D., Özkan-Altıner, S., Okay, N., 2012. An olistostrome–mélange belt formed along a suture: Bornova Flysch zone, western Turkey. Tectonophysics 568–569, 282–295.
Özkaymak, Ç., Sözbilir, H., Uzel, B., 2013. Neogene–Quaternary evolution of the Manisa Basin: evidence for variation in the stress pattern of the İzmir–Balıkesir Transfer Zone, western Anatolia. J. Geodyn. 65, 117–135.
Peccerillo, A., Taylor, S.R., 1976. Geochemistry of Eocene calc-alkaline volcanic rocks from the Kastamonu area, northern Turkey. Contrib. Mineral. Petrol. 58, 63–81.
Pécskay, Z., Lexa, J., Szakács, A., Seghedi, I., Balogh, K., Konečný, V., Zelenka, T., Kovacs, M., Póka, T., Fülöp, A., Márton, E., Panaiotu, C., Cvetković, V., 2006. Geochronology of Neogene magmatism in the Carpathian arc and intra-Carpathian area: a review. Geol. Carpath. 57, 511–530.
Pe-Piper, G., Piper, D.J.W., Matarangas, D., 2002. Regional implications of geochemistry and style of emplacement of Miocene I-type diorite and granite, Delos, Cyclades, Greece. Lithos 60, 47–66.
Prelević, D., Akal, C., Romer, R.L., Foley, F., 2010. Lamproites as indicators of accretion and/or shallow subduction in the assembly of Southwestern Anatolia, Turkey. Terra Nova 22, 443–452.
Prelević, D., Akal, C., Foley, S.F., Romer, R.L., Stracke, A., Van Den Bogaard, P., 2012. Ultrapotassic mafic rocks as geochemical proxies for post-collisional dynamics of orogenic lithospheric mantle: the case of southwestern Anatolia, Turkey. J. Petrol. 53, 1019–1055.
Rudnick, R.L., Fountain, D.M., 1995. Nature and composition of the continental crust — a lower crustal perspective. Rev. Geophys. 33, 267–309.
Savaşçın, M.Y., 1978. Mineralogical and geochemical investigations and source interpretations of Foça-Urla Neogene Volcanites (in Turkish). pp. 1–15 (PhD. Thesis).
Sayılı, İ.S., Gonca, Ş., 1999. İzmir–Karşıyaka Altıntepe ve Çilektepe sektörlerinin jeolojisi, petrografisi ve diğer metal cevherleşmeleri. MTA Derg. 121, 199–215 (Geology, petrography and precious metal formations in the İzmir–Karşıyaka Altıntepe area and Çilektepe section. MTA Dergisi 121, 199–215).
Schumm, S.A., Dumont, J.F., Holbrook, J.M., 2000. Active Tectonics and Alluvial Rivers. Cambridge University Press (276 pp.).
Seghedi, I., Downes, H., 2011. Geochemistry and tectonic development of Cenozoic magmatism in the Carpathian–Pannonian region. Gondwana Res. 20, 655–672.
Seghedi, I., Szakács, A., Roşu, E., Pécskay, Z., Gméling, K., 2010. Note on the evolution of a Miocene composite volcano in an extensional setting, Zărand Basin (Apuseni Mts., Romania). Cent. Eur. J. Geosci. 2, 321–328.
Seghedi, I., Ersoy, Y.E., Helvacı, C., 2013. Miocene–Quaternary volcanism and geodynamic evolution in the Pannonian Basin and the Menderes Massif: a comparative study. Lithos 180–181, 25–42.
Seyitoğlu, G., Anderson, D., Nowell, G., Scott, B., 1997. The evolution from Miocene potassic to Quaternary sodic magmatism in Western Turkey: implications for enrichment processes in the lithospheric mantle. J. Volcanol. Geotherm. Res. 76, 127–147.
Sherlock, S., Kelley, S., Inger, S., Harris, N., Okay, A., 1999. ^{40}Ar–^{39}Ar and Rb–Sr geochronology of high-pressure metamorphism and exhumation history of the Tavsanli Zone, NW Turkey. Contrib. Mineral. Petrol. 137, 46–58.
Singer, B.S., Leeman, W.P., Thirlwall, M.F., Roger, N.W.E., 1996. Does fracture zone subduction increase sediment flux and mantle melting in subduction zones? Trace element evidence from Aleutian arc basalt. In: Bebout, G.E., Scholl, D.W., Kirby, S.H., Platt, J.P. (Eds.), Subduction Top to Bottom. Geophysical Monograph vol. 96, pp. 285–291.
Sözbilir, H., Sarı, B., Uzel, B., Sümer, Ö., Akkiraz, S., 2011. Tectonic implications of transtensional supradetachment basin development in an extension-parallel transfer zone: the Kocaçay Basin, western Anatolia, Turkey. Basin Res. 23, 423–448.
Steiger, R.H., Jäger, E., 1977. Subcommisssion on geochronology: convention on the use of decay constants in geo- and cosmochronology. Earth Planet. Sci. Lett. 12, 359–362.
Sun, S., McDonough, W.F., 1989. Chemical and isotopic systematics of oceanic basalts: implications for mantle compositions and processes. Geochem. Soc. Spec. Publ. 42, 313–345.
Thirlwall, M.F., Smith, T.E., Graham, A.M., Theodorou, N., Hollings, J.P., Davidson, J.P., Arculus, R.J., 1994. High field strength element anomalies in arc lavas: source or process? J. Petrol. 35, 819–838.
Tibaldi, A., Bistacchi, A., Pasquarè, F., Vezzoli, L., 2006. Extensional tectonics and volcano lateral collapses: ınsight from Ollag e volcano (Chile) and analogue modelling. Terra Nova 18, 158–170.
Uzel, B., Sözbilir, H., 2008. A first record of strike-slip basin in western Anatolia and its tectonic implication: the Cumaovası basin as an example. Turk. J. Earth Sci. 17, 559–591.
Uzel, B., Sözbilir, H., Özkaymak, Ç., Kaymakcı, N., Langereis, C.G., 2013. Structural evidence for strike-slip deformation in the İzmir–Balıkesir transfer zone and consequences for late Cenozoic evolution of western Anatolia (Turkey). J. Geodyn. 65, 94–116.
Yılmaz, Y., Genç, Ş.C., Gürer, F., Bozcu, M., Yılmaz, K., Karacık, Z., Altunkaynak, Ş., Elmas, A., 2000. When did the western Anatolian grabens begin to develop? In: Bozkurt, E., Winchester, J.A., Piper, J.D.A. (Eds.), Tectonics and Magmatism in Turkey and the Surrounding Area. The Geological Society of London 173. Special Publications, London, pp. 353–384